

CrossMark
click for updatesCite this: *RSC Adv.*, 2016, 6, 87935

Dual drug-loaded halloysite hybrid-based glycocluster for sustained release of hydrophobic molecules†

M. Massaro,^a S. Riela,^{*a} C. Baiamonte,^b J. L. J. Blanco,^c C. Giordano,^b P. Lo Meo,^a S. Milioto,^d R. Noto,^a F. Parisi,^d G. Pizzolanti^b and G. Lazzara^{*d}

A dual drug-loaded HNT-CD glycocluster delivery system based on halloysite nanotubes and carbohydrate functionalized cyclodextrin was developed by a green protocol using solvent-free microwave irradiation. The nanohybrid was employed for concurrent load and release of silibinin and curcumin. The new delivery system was characterized by means of TGA, FT-IR spectroscopy, SEM and DLS. These techniques confirm the successful loading of the two drugs in the system. SEM and DLS measurements highlighted that the nanomaterial preserves a tubular structure with an average hydrodynamic radius of ca. 200 nm. The release of the drugs from the HNT glycocluster was investigated by means of UV-vis spectroscopy at two different pH values simulating the typical physiological conditions of either gastric or intestinal fluids. Enzyme-linked lectin assays (ELLA) demonstrated that highly mannoside-cyclodextrins HNT entities display high affinity towards mannoside selective ConA lectin. Biological assays showed that the new drug delivery system exhibits anti-proliferative activity against the investigated cell lines. Fluorescence microscopy confirmed ELLA results and it showed a high propensity of this drug delivery system to cross cell membranes and to penetrate into the cell nucleus. The results revealed that the synthesized multicavity system is a material of suitable size and nanoarchitecture to transport drugs into living cells.

Received 6th June 2016

Accepted 8th September 2016

DOI: 10.1039/c6ra14657k

www.rsc.org/advances

Introduction

Nanomedicine, based on nanomaterials as drug delivery systems (DDS), provides the opportunity to design multilevel molecular aggregates that have novel functional and dynamic properties desirable for therapeutic applications. Drug delivery to specific targets has become an important issue for promoting the selectivity of drugs to diseased sites and reducing toxicity against normal cells thanks to the ability of the nanocarrier in overcoming various biological barriers and localizing in target tissue.¹

In the last year many studies have focused on the combination of two or more therapeutic drugs to achieve a synergistic effect at lower drug doses in cancer treatment.² In principle, the

co-administration of two or more drugs, with different physicochemical properties and action mechanisms, maximizes therapeutic efficacy and overcomes drug resistance.³

In recent years, various nanomaterials have been employed for the design of high performance drug carriers.⁴ Among them halloysite is a very interesting natural mineral due to its peculiar hollow tubular structure, with an outer diameter of 40–70 nm, an inner diameter of 10–20 nm and a length of 500–1000 nm,⁵ consisting of silica on the outer surface and alumina at the innermost surface.^{6–8} Halloysite is a bio and eco-compatible materials as shown by several *in vitro* and *in vivo* studies.^{9–14} The empty halloysite lumen makes it an efficient container for load and release of hydrophobic molecules,¹⁵ and provides at the same time the possibility to modify either surfaces to realize intelligent nanoscale materials.⁸ Release from the HNT lumen usually occurs from several hours to days depending on structure, molecular weight and solubility of the agents in the release medium. The use of halloysite as nano-container for drug loading and release was firstly introduced by Price, Gaber and Lvov.¹⁶ Up to day, several examples are reported about HNT drug carrier systems.¹⁷ The halloysite toxicity has extensively been evaluated both *in vitro* using human cell cultures and *in vivo* employing protists and microscopic worms. Each study performed highlighted that although halloysite can be easily taken up by the cultured cells, accumulating predominantly near its perinuclear region, its toxicity was reported to be very low.¹⁸

^aDipartimento STEBICEF, Sez. Chimica, Università degli Studi di Palermo, Viale delle Scienze, Parco d'Orleans II, Ed. 17, 90128 Palermo, Italy. E-mail: serena.riela@unipa.it; Tel: +39-09123897546

^bDipartimento Biomedico di Medicina Interna e Specialistica, Sez. Endocrinologia, Diabetologia, Metabolismo, Università degli Studi di Palermo, 90127 Palermo, Italy

^cDepartment of Organic Chemistry, Faculty of Chemistry, University of Sevilla, E-41012 Sevilla, Spain

^dDipartimento di Fisica e Chimica, Università degli Studi di Palermo, Viale delle Scienze, Parco d'Orleans II, Ed. 17, 90128 Palermo, Italy. E-mail: giuseppe.lazzara@unipa.it

† Electronic supplementary information (ESI) available: Experimental details, FT-IR spectra, TGA curves, cell viability. See DOI: 10.1039/c6ra14657k

HNTs have been used in the nanoscale drug delivery systems of quercetin,¹⁹ ibuprofen,²⁰ diclofenac sodium,²¹ curcumin,²² brilliant green,²³ salicylic acid²⁴ and so on,^{25,26} which all focused on its inherent lumen. Recently Zhou *et al.* reported a dual-DDS comprising poly(L-lactide)/HNTs electrospun mats capable of co-delivering hydrophilic and hydrophobic drugs.²⁷ The nanomaterial exhibited considerable antibacterial activity and put forward the use of halloysite as wound-dressing materials. Two different flavonoids were simultaneously loaded on HNT based carriers and the dual-drug system showed enhanced anti-proliferative activity compared to the free drugs on human cancer cells.²⁸ Moreover, synergistic antitumoral effects were observed in triazolium salts–HNT prodrug systems loaded with biological active molecules such as curcumin and cardanol.^{29,30} However, the development of drug carrier systems that simultaneously load different drugs showing sustained release, remains a challenge. Modification of the HNT surfaces with targeting ligands such as peptides, antibodies, folic acid and aptamers, affords materials which specifically bind to the receptors overexpressed only in cancer cells (“active targeting”).³¹ Among them, carbohydrates, which exhibit selective binding affinity to lectins present on the cellular surface, have been extensively tested in order to facilitate the targeted delivery of drugs.³² Since the dissociation constants of carbohydrate–lectin complexes are in the millimolar range, multivalent systems (which involve the simultaneous binding of multiple

ligands onto multiple receptors) are required for efficient recognition (glycocluster effect).³³

The aim of this study is to fabricate and to characterize a dual-drug loaded HNT delivery system (Fig. 1). The possibility of delivery two drugs is achieved by the introduction of a second cavity by covalent linkage of β -cyclodextrin (β CD) units on HNT external surface. Targeting functionalities as well as glycocluster effect were introduced by attaching on the β CD core mannose units. To verify if the obtained system is able to mimic the typical lectin–carbohydrate interactions occurring on the cell wall, we have investigated the affinity towards α -Man-specific lectin concanavalin A (ConA) by competitive enzyme-linked lectin assay (ELLA). The controlled pH triggered release of the drugs from the dual-drug loaded HNT system was also evaluated. Eventually, the efficacy of this delivery system was tested for tumor growth inhibition against 8505c thyroid cancer cell line and the interaction with them was explored by fluorescence microscopy.

Results and discussion

Schematic representation of synthetic route to obtain halloysite nanotube–cyclodextrin hybrids loaded with silibinin and curcumin is depicted in Fig. 2.

Synthesis and characterization of HNT–CD delivery system

The fabrication of a halloysite-functionalized CD material has been successfully carried out by means of solvent-free microwave irradiation techniques as previously reported.³⁴ In particular, thiol functionalized halloysite was reacted with heptakis-6-(*tert*-butyldi-methylsilyl)-2-allyloxy- β -cyclodextrin under microwave irradiation for 1 h, at 100 °C. Then, the obtained material was further functionalized by decorating the secondary rim of CD units with thiomannoside units (Fig. 3); this strategy afforded a nanomaterial with 1.5 wt% of mannose units, as estimated by thermogravimetric analysis (TGA).³⁴

Since ConA, one of the most abundant carbohydrate binding proteins, exhibits higher selectivity to α -mannose configuration than to the β one, the mannose probe is designed to possess the α -glycosidic linkage. Furthermore, in order to push the sugar probe away from the HNT–cyclodextrin hindrance, we have also

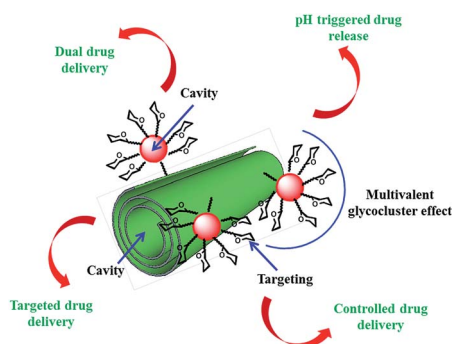


Fig. 1 HNT–CD glycocluster system.

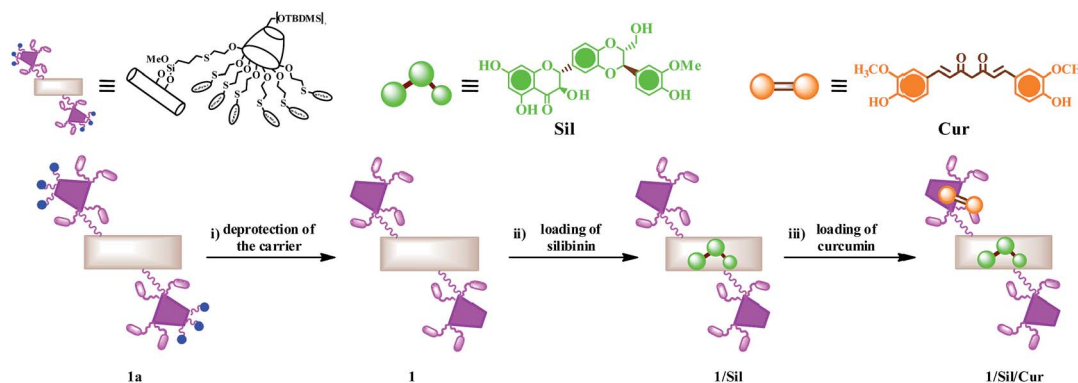


Fig. 2 Schematic representation of synthetic route to halloysite nanotube–cyclodextrin hybrids loaded with silibinin and curcumin.

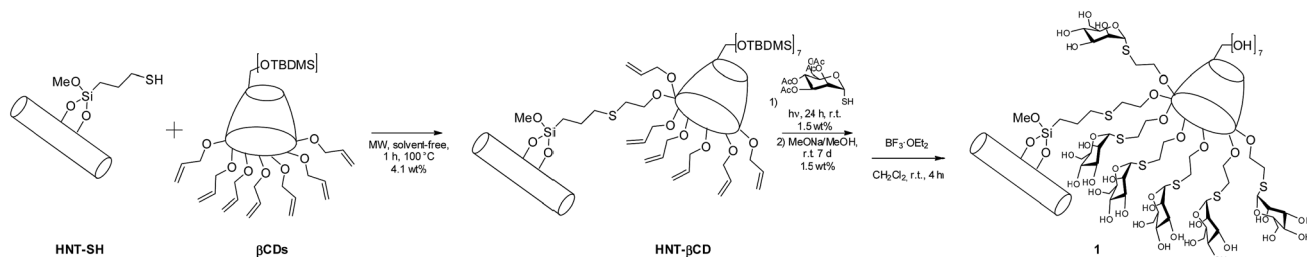


Fig. 3 Synthesis of compound 1.

used an alkylic spacer to increase the flexibility of the immobilized ligand.

Compound **1** was obtained by deprotecting the hydroxyl groups of the primary rim of cyclodextrin present in **1a**. The deprotection reaction was a crucial step to obtain the final material because the siloxane external surface of HNT is destroyed under the common experimental conditions adopted to remove the TBDMS groups (2 eq. of tetra-*n*-butylammonium fluoride (TBAF), for each cyclodextrin core, in tetrahydrofuran (THF)). The protective group was, successfully, removed with $\text{BF}_3 \cdot \text{OEt}_2$ at rt for 4 h. Under these particular conditions no degradation of HNT occurred.

Development of the dual drug-loaded HNT-CD delivery system

The presence of two cavities in compound **1** offers the remarkable possibility for a simultaneous encapsulation and co-delivery of two different molecules. As drug models were chosen silibinin and curcumin, that have been shown *in vitro* to be potentially active agents towards several tumor cell lines.^{35–37}

Previous studies showed that curcumin is able to interact both with HNT lumen and cyclodextrin cavity;³⁴ whereas silibinin can be loaded into HNT lumen only.²⁸

Therefore, in order to achieve the highest loading of silibinin and curcumin on **1**, we load first silibinin and then curcumin. Loading of silibinin into **1** was carried out by vacuum cycling of a suspension of **1** in a saturated silibinin solution. This cycle was repeated three times in order to obtain the highest loading efficiency. After loading, the **1**/Sil complex was washed in order to remove the free silibinin. **1**/Sil was suspended again in water and then, to this dispersion a saturated solution of curcumin was added. Subsequent investigations were conducted on the dry solid filtered from dispersion, washed with water and dried overnight at 60 °C.

The loading efficiencies of HNT/Sil and HNT/Sil/Cur were estimated spectrophotometrically. The amount of Sil loaded in the HNT lumen and Cur encapsulated into CD cavity, expressed as the percent amount of drug in the final composite, was *ca.* 2.5 wt% for both molecules with encapsulation efficiencies of 93% and 66% for silibinin and curcumin, respectively.

The FT-IR spectrum of the solid complex showed the disappearance of the C=O and C=C stretching bands at 1628, 1605 and 1509 cm^{-1} of curcumin (Fig. 4). Given that the presence of Cur is proved straightforwardly by TGA and UV-vis

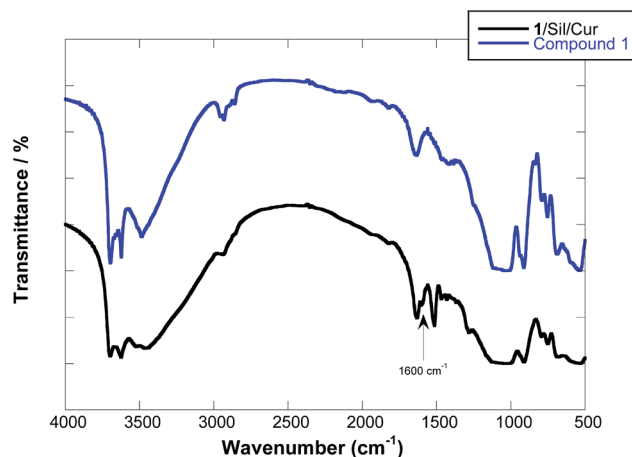


Fig. 4 FT-IR spectra of compound **1** and **1**/Sil/Cur complex.

spectra (see below), such bands missing indicate the occurrence of deep structural changes for Cur upon formation of the solid complex with the HNT glycocluster. It was hypothesized that curcumin interact with cyclodextrin cavity forming a 1 : 2 complex in which a single Cur unit bridges two HNT-cyclodextrin and consequently loss of its spectral properties.³⁴

Therefore, the new peaks that one can observe in **1**/Sil/Cur are related to silibinin, in particular C=O stretching vibration band (at 1600 cm^{-1}) related to the carbonyl group of silibinin (see ESI†), which is shifted to lower frequencies with respect to pure silibinin (1638 cm^{-1}). A similar effect was evidenced for cetyltrimethyl ammonium bromide³⁸ and cucurbit[8]uril adsorption³⁹ onto HNT and it was related to the high packing density of organic moiety at the interface.⁴⁰ Accordingly, the shifting of the stretching bands could be ascribed to the electrostatic interactions between the positively alumina groups of HNTs inner surface and the dipole of carbonyl and hydroxyl groups of silibinin.

The composite solids **1**/Sil and **1**/Sil/Cur were characterized by TGA. The thermoanalytical curves clearly show that after each loading step a systematic decrease in the residual mass at 900 °C occurs. This result is consistent with the entrapment of the organic drug into compound **1** (Fig. 5). To better highlight the degradation of loaded drug into the composite material, the difference of the TG curves are plotted (see ESI†). It might be noted that in **1**/Sil the degradation curves is reminiscent of

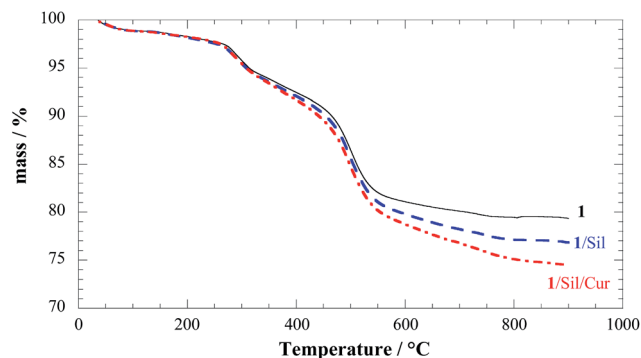


Fig. 5 Thermoanalytical curves for compound **1** before and after loading with silibinin and curcumin.

those for pure silibinin showing a slow degradation process in a wide temperature range (see ESI†).

It is also interesting to note that silibinin was thermally stabilized by loading into HNTs, as its thermal degradation curve was shifted toward higher temperature as compared to the native molecule.²⁸ This enhancement of the thermal stability can be due to encapsulation of the degradation products into the nanotube lumen and confirm the inclusion of silibinin in HNT lumen.⁴¹

Moreover, for the complex **1**/Sil/Cur an additional degradation step between 300 °C and 450 °C is consistent with the degradation feature of free curcumin; therefore on this basis it can rule out the inclusion into the HNT lumen and the specific interaction with β CD cavity.³⁴ Given that both silibinin and curcumin degraded with a null residual at 900 °C, we calculated that compound **1** is able to incorporate 2.6% of silibinin and 2.4% of curcumin in agreement with UV-vis results. These results prove that the modified HNTs with a double cavity are efficient as nano-container for co-delivery of two biological active molecules.

The morphology and the diffusion dynamics in water of the complex **1**/Sil/Cur were characterized by scanning electron microscopy (SEM) and dynamic light scattering (DLS).

SEM images show that the tubular shape of the nanoclay is not lost after the new proposed protocol for deprotection of the hydroxyl groups on primary rim of cyclodextrin. Comparing the SEM images of the complex with that of the pristine material,³⁴ we can conclude that the average characteristic sizes of the nanoparticle are not altered (Fig. 6). Measurements of the particle size using DLS revealed an apparent hydrodynamic radius of 115 nm for the complex. Previous studies have shown that the size of therapeutic nano-platform could affect the ability of deep tissue penetration and cancer cell internalization, and further impact the efficacy of nanomedicine.⁴² The average hydrodynamic size of **1**/Sil/Cur is in the range of ~20–200 nm, which is expected to avoid renal filtration, leading to prolonged residence time in the body that enables more effective targeting of diseased tissue.⁴³

pH triggered release of biological molecules from **1**

The controlled release of Cur and Sil from the complexes **1**/Sil/Cur was studied in aqueous buffers at both pH 1.0 and 7.4, *i.e.*

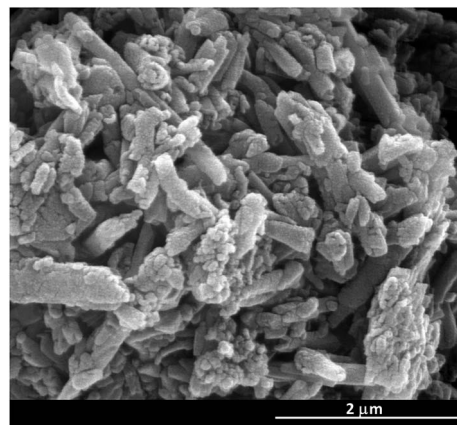


Fig. 6 SEM images of the complex **1**/Sil/Cur.

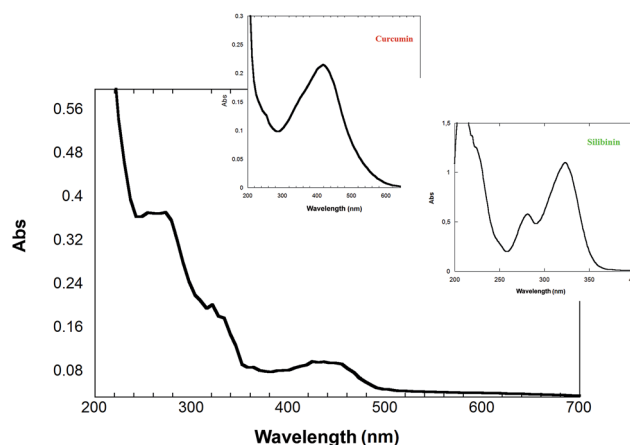


Fig. 7 UV-vis spectra of curcumin and silibinin released from **1** at pH 7.4. The insets show the spectra of silibinin and curcumin.

in such a way to mimic the typical physiological conditions of either gastric or intestinal fluids. The Cur and Sil release profiles were determined under different conditions by a membrane dialysis method using UV-vis spectrophotometry. In particular the two drugs show well distinguished absorption maxima in the investigated pH range. As proved in Fig. 7 the drugs preserved their spectral properties after release.

The extended release profiles of silibinin and curcumin from **1**, at both pH were elucidated (Fig. 8).

In both media, silibinin was released in a greater amount than curcumin.

As it is possible to note, the release of silibinin at pH 1.0 from compound **1** showed an initial burst within 200 min followed by a prolonged release. The release profile obtained at pH 7.4 reaches a plateau after 400 min and showed a small amount of silibinin released from the system. As it can be seen there are significant differences for the release in different pH conditions, which can be explained as follows. In acidic solution both **1** and silibinin are positively charged; therefore, electrostatic repulsions may also accelerate the release of drug from **1**. On the contrary, in physiological medium silibinin

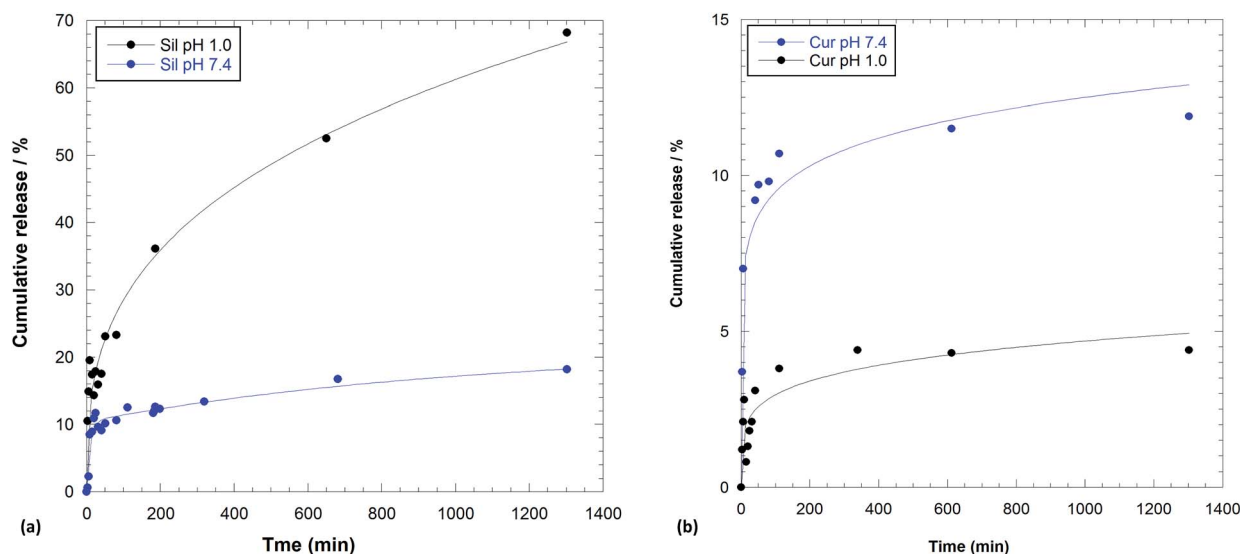


Fig. 8 Amount of (a) silibinin and (b) curcumin released from 1 in 0.1 M HCl solution and phosphate buffer pH 7.4.

could be partially dissociated, consequently it is less soluble in aqueous medium and therefore a small release of silibinin occurred.

Release profile obtained for curcumin at both pH showed a similar behavior than silibinin, but in this case a very low amount of molecules was released from the system (Fig. 8b).

The different curcumin release in the two media could be explained taking into account the affinity, in different pH range, of the molecule for cyclodextrin cavity.

The small amount of curcumin released from 1 at pH 1.0 could be explained on the basis of a strong interaction of the molecules and CD cavity in acidic medium;⁴⁴ with the increasing pH value, the affinity between curcumin and cyclodextrin was decreased.⁴⁵

These results demonstrated that Sil and Cur in the 1/Sil/Cur displayed a sustained and long-term release profile, with a total amount of Sil and Cur released being about 23% and 5%, respectively, within 60 min and 65% and 5% respectively, after 400 min in acidic solution. On the contrary, 10% of both molecules within 60 min and 13% and 12% of Sil and Cur respectively in physiological condition were released. In the 1/Sil/Cur release system, the lower release amount of curcumin in the simulated gastric fluid, whereas more rapid release rate (Table 1) and higher release amount in the simulated intestinal fluid could be advantageous for actual application to maintain

effective concentration in the body and reduce the maximum extent of the side effects to the stomach.

In order to better understand the release behavior of silibinin and curcumin under different pH conditions, the *in vitro* release data were fitted to two models to analyze the kinetics and the release mechanism of both molecules. The experimental data were analyzed using double exponential model (DEM)⁴⁶ and the power law (Table 1).⁴⁷ The results showed that the release of silibinin at pH 1.0 and curcumin at both pH values follow the power fit model (R^2 higher than 0.97) with a “ n ” value lower than 0.5 in all cases, indicating that biological molecules release was controlled by a drug diffusion process. It was found that the release mode of silibinin in neutral solution follows the double exponential model. According to the literature, the DEM describes a mechanism consisting of two parallel reactions involving two distinguishable species.²⁸ In our particular case we observed the release of silibinin and the simultaneous release of curcumin that, in physiological medium presents a maximum absorption at 260 nm close to the one of silibinin in this pH range.

Target drug delivery: enzyme-linked lectin assays (ELLA)

ELLA measures the ability of a ligand to inhibit the association between a labelled lectin and a polymeric ligand attached to the

Table 1 Kinetic parameters for the release of silibinin and curcumin from 2 in pH and pH 7.4 solution

| | pH | DEM | | | Power fit | | |
|-----|-----|----------------------------|-----------------------------|-------|---------------------------|-------|-----------------|
| | | k' (min^{-1}) | k'' (min^{-1}) | R^2 | k (min^{-1}) | R^2 | n |
| Sil | 1 | — | — | — | 5.9 ± 0.5 | 0.98 | 0.34 ± 0.01 |
| Cur | 1 | — | — | — | 1.4 ± 0.4 | 0.98 | 0.28 ± 0.04 |
| Sil | 7.4 | 0.11 ± 0.03 | 0.002 ± 0.001 | 0.96 | 4.3 ± 1.6 | 0.88 | 0.21 ± 0.05 |
| Cur | 7.4 | — | — | — | 4.2 ± 0.9 | 0.97 | 0.21 ± 0.03 |

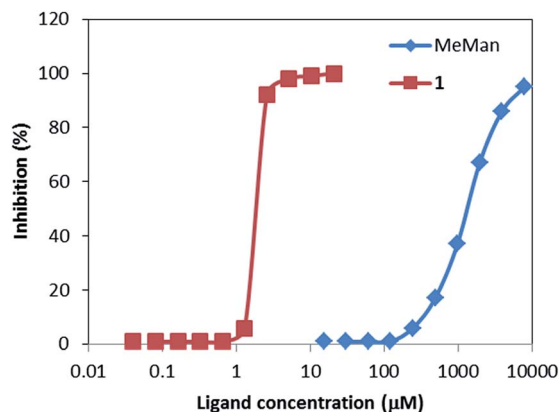


Fig. 9 ELLA affinity curves of α -MeMan (blue line, starting concentration 7725 μ M) and **1** (red line, starting concentration 20.5 μ M). IC_{50} MeMan = 1300 μ M and IC_{50} **1** = 1.9 μ M. The IC_{50} are mean values obtained from at least three estimations, within a $\pm 15\%$ error.

microtiter well (horseradish peroxidase-labelled ConA and yeast mannan, respectively, in the present case). The concentration needed to achieve 50% inhibition (IC_{50}) is then assumed to be inversely proportional to the lectin-saccharide free energy of binding.

The experimental ELLA data are summarized in Fig. 9. Highly dense glycocluster **1** featured a remarkable cluster effect. Comparison of IC_{50} (1300 μ M) value of α -Me-mannoside with **1** IC_{50} (1.9 μ M) concentration demonstrated that highly mannoside-cyclodextrins HNT entities display high affinity towards mannose selective ConA lectin. Consequently, the cluster effect of compound **1** has increased approximately 700-fold the relative potency of **1** compound respect to α -Me-mannoside which means 100-fold more affinity per mannose unit. These results are in agreement with previous studies on highly mannosylated cyclodextrins clusters in which a 21-mannoside cyclodextrin derivative displayed ~ 160 -fold relative potency.³³

Tumor growth inhibition: MTS test

Anaplastic thyroid cancer (ATC) is one of the most aggressive malignancies in humans. ATC is highly resistant to standard therapeutic interventions, including surgical treatment, radiation therapy and chemotherapy.⁴⁸

We have tested the potential anti-proliferative activity *in vitro* of the **1**/Sil/Cur complex on an ATC cell line 8505c by means MTS tests. The survival rates of both cell lines incubated with **1** at different concentrations were found in the range of 96–100%, indicating that they have no effect on cell viability. Free curcumin and silibinin have no effect on cell viability, probably due to their insolubility in physiological medium (see ESI†).

The 8505c cell line showed dose dependent cytotoxic profile when exposed to **1**/Sil/Cur complex (Fig. 10). After 72 h of drug exposure, **1**/Sil/Cur exhibited an excellent cytotoxicity activity against 8505c, with an IC_{50} value of 11.3 ± 3.1 μ M. This excellent toxicity exerted by the synthesized complex could be explained by a synergic effect deriving of the co-administration of curcumin and silibinin.

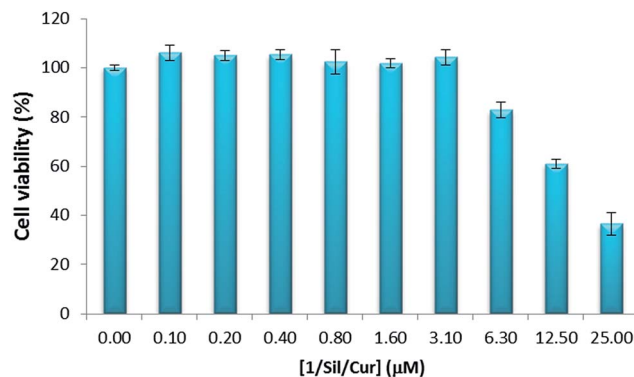


Fig. 10 MTS test for cell viability of 8505c cells cultured for 72 h in presence of **1**/Sil/Cur. The data are mean values obtained from at least three estimations.

In addition, the IC_{50} value could suggest that the carbohydrate-receptor-mediated endocytosis with targeting specificity led to greater cellular uptake of the drugs and therefore killed the cancer cells more efficiently than similar halloysite-cyclodextrin hybrids without targeting ligand (IC_{50} of $27.6 \mu\text{M} \pm 6$).²⁸

These findings result particularly important when considering that, at present, there is no efficient chemotherapeutic drug against ATC and survival of patients is less than 1 year.⁴⁸

Cellular uptake

To evaluate the potential application of **1**/Sil/Cur as novel drug delivery system, the uptake and localization into 8505c thyroid cancer cell lines of **1**/Sil/Cur was performed. We analyzed, the interaction between cells and the dual drug-loaded HNT-CD system by means of fluorescence microscopy. The data revealed that **1**/Sil/Cur complex showed a high propensity to cross cell membranes and this nanodrug delivery system is able to penetrate in the cell nucleus as highlighted by the silibinin fluorescence emission (green) localized in the nuclei (Fig. 11). The results suggested that the **1**/Sil/Cur complexes could effectively transport into living cells.

These findings are in agreement with the data obtained from ELLA test and highlight the importance of the sugars onto the

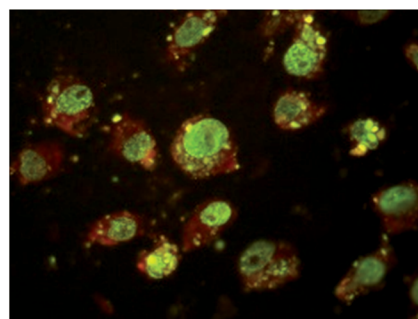


Fig. 11 Fluorescence microscope images of the **1** uptake by 8505C. 8505C cell membrane (red) with co-localized **1** (green) inside nuclei at 24 h.

carrier surface. Similar tests performed on the same cell line in the presence of halloysite–cyclodextrin hybrids without sugar moieties revealed that the green fluorescence, associated with the fluorescence of the nanoparticles, was observed in the cytoplasm but not in the nucleus.²⁸

Experimental

Materials and methods

All needed reagents were used as purchased (Aldrich), without further purification.

Cyclodextrin functionalized HNTs were prepared according to previous report.³⁴

Thermogravimetric analyses were performed on a Q5000 IR apparatus (TA Instruments) under a nitrogen flow of 25 cm³ min⁻¹ for the sample and 10 cm³ min⁻¹ for the balance. The weight of each sample was *ca.* 10 mg. Measurements were carried out by heating the sample from rt up to 900 °C at a rate of 10 °C min⁻¹.

FT-IR spectra (KBr) were recorded using an Agilent Technologies Cary 630 FT-IR spectrometer. Specimens for measurements were prepared by mixing 5 mg of the sample powder with 100 mg of KBr.

Dynamic light scattering (DLS) experiments were done by means of a Zetasizer NANO-ZS (Malvern Instruments). The field-time autocorrelation functions were well described by a single decay, which provides the decay rate (Γ) of the diffusive mode. For the translational motion, the collective diffusion coefficient at a given concentration is $D_t = \Gamma/q^2$ where q is the scattering vector given by $4\pi n\lambda^{-1} \sin(\theta/2)$ being n the water refractive index, λ the wavelength (632.8 nm) and θ the scattering angle (173°). The apparent hydrodynamic radius was calculated by means of Stokes–Einstein equation.

A microscope ESEM FEI QUANTA was used to study the morphology. The sample was coated with gold in argon by means of an Edwards Sputter Coater S150A to avoid charging under electron beam.

UV-vis measurements were performed using a Beckmann DU 650 spectrometer.

Deprotection of hydroxyl groups of cyclodextrin

In a 25 mL round bottom flask compound **1a** (200 mg) was weighed, and 7.5 mL of CH₂Cl₂ were added under constant stirring and argon atmosphere. Then BF₃·OEt₂ (35 μL) was added dropwise at the dispersion. The reaction mixture was stirred at room temperature for 4 hours. The dispersion was then filtered off rinsed with water and dried overnight *in vacuo* at 70 °C.

Loading of silibinin and curcumin

To a dispersion of **1** in deionized water (5 mL), 1 mL of silibinin solution 10⁻² M in ethanol was added. The suspension was sonicated for 5 min, at an ultrasound power of 200 W and at 25 °C and then was evacuated for 3 cycles. The suspension was left under stirring for 24 h at room temperature. After this time the powder was washed with water and then dried at 60 °C under

vacuum. Afterwards the 1/Sil solid complex was suspended again in deionized water (5 mL) and 1 mL of curcumin solution (10⁻² M) in ethanol was, then, added. The suspension was stirred for 24 h at rt and then was filtered; the powder was washed with small amounts of water and then dried at 70 °C under vacuum overnight. The loading efficiency was calculated according to the original concentration of Sil and Cur and the concentration of unloaded molecules quantified by means of UV-vis spectrophotometry at the monitoring wavelengths of 280 and 420 nm for silibinin and curcumin, respectively. The loading percentages of Sil and Cur into HNT lumen and CD cavity were also calculated by dividing the mass of the encapsulated molecules by the mass of the molecules-loaded HNT–cyclodextrin powder.

Drug encapsulation efficiencies (EE) were determined with the following equation:

$$EE = \left(\frac{\text{actual loading}}{\text{theoretical loading}} \right) \times 100 \quad (1)$$

Kinetic release

The release of curcumin and silibinin from the 1/Sil/Cur complexes was performing as follows: 25 mg of the sample were dispersed in 1 mL of dissolution medium and transferred into a dialysis membrane (Medicell International Ltd MWCO 12–14 000 with diameter of 21.5 mm). The membrane was then put in a round bottom flask containing 10 mL of the release medium at 37 °C and stirred.

Two different media (0.1 M HCl and phosphate buffer pH 7.4, respectively) were considered in order to evaluate the influence of pH on the release behavior of the drug.

At fixed times, 1 mL of the release medium was withdrawn and analyzed. To keep constant the volume of the release medium 1 mL of fresh solution (0.1 M HCl, pH 7.4 buffer) was added each time to replace the withdrawn one.

The curcumin and silibinin concentrations in the solution were determined by UV-vis spectrophotometry using the Lambert–Beer law.

Total amounts of drug released (F_t) were calculated as follows:

$$F_t = V_m C_t + \sum_{i=0}^{t-1} V_a C_i \quad (2)$$

where V_m and C_t are volume and concentration of the drug at time t . V_a is the volume of the sample withdrawn and C_i is drug concentration at time i ($i < t$).

To determine the release mechanism, the amount of released molecules *vs.* time was studied using the following mathematical models:

$$F_t = F_e(1 - e^{-k't}) + F''_e(1 - e^{-k''t}) \quad (3)$$

$$F_t = kt^n \quad (4)$$

where F_t is the drug release fraction at time t , k is the kinetic release constant of the respective equations, t is the release time

and n is the characteristic diffusion exponent, depending on the release mechanism and the geometry of device. If Fickian diffusion occurred, n decreased to 0.5 for slab/cylinder/sphere. If non-Fickian (anomalous) diffusion dominated, the n value was between the above value corresponding to the polymer chain relaxation ($n < 1$) for slab/cylinder/sphere. Thus, through determination of the n value, the drugs release mechanism could be identified.

Enzyme-linked lectin assay (ELLA)

Nunc-Immuno™ plates (MaxiSorp™) were coated overnight with yeast mannan at 100 mL per well diluted from a stock solution of 10 mg mL⁻¹ in 0.01 M phosphate buffer saline (PBS, pH 7.3 containing 0.1 mM Ca²⁺ and 0.1 mM Mn²⁺) at room temperature. The wells were then washed three times with 300 mL of washing buffer (containing 0.05% (v/v) Tween 20) (PBST). The washing procedure was repeated after each of the incubations throughout the assay. The wells were then blocked with 150 mL per well of 1% BSA/PBS for 1 h at 37 °C. After washing, the wells were filled with 100 mL of serial dilutions of horse-radish peroxidase labelled concanavalin A (ConA-HRP) from 10⁻¹ to 10⁻⁵ mg mL⁻¹ in PBS, and incubated at 37 °C for 1 h. The plates were washed and 50 mL per well of 2,2'-azinobis-(3-ethylbenzothiazoline-6-sulfonic acid)diammonium salt (ABTS) (0.25 mg mL⁻¹) in citrate buffer (0.2 M, pH 4.0 with 0.015% H₂O₂) was added. The reaction was stopped after 20 min by adding 50 mL per well of 1 M H₂SO₄ and the absorbances were measured at 415 nm. Blank wells contained citrate-phosphate buffer. The concentration of lectin-enzyme conjugate that displayed an absorbance between 0.8 and 1.0 was used for inhibition experiments.

In order to carry out the inhibition experiments, each inhibitor was added in a serial of 2-fold dilutions (60 mL per well) in PBS with 60 mL of the desired ConA-peroxidase conjugate concentration on Nunclon™ (Delta) microtiter plates and incubated for 1 h at 37 °C. The above solutions (100 mL) were then transferred to the mannan-coated microplates, which were incubated for 1 h at 37 °C. The plates were washed and the ABTS substrate was added (50 mL per well). Color development was stopped after 20 min and the absorbances were measured. The percent of inhibition was calculated as follows:

$$\% \text{ inhibition} = \frac{A_{\text{no inhibitor}} - A_{\text{with inhibitor}}}{A_{\text{no inhibitor}}} \quad (5)$$

Results in triplicate were used for plotting the inhibition curves for each individual ELLA experiment. Typically, the IC₅₀ values (concentration required for 50% inhibition of the ConA coating mannan association) obtained from several independently performed tests were in the range of $\pm 15\%$. Nevertheless, the relative inhibition values calculated from independent series of data were highly reproducible.

Cell culture

The human anaplastic thyroid carcinoma cell line 8505c was from ECACC (Sigma-Aldrich, Milan, Italy) and cultured in RPMI

1640 (PAA, Pasching Austria) supplemented with 10% FBS (Sigma-Aldrich, Milan, Italy). The human anaplastic thyroid carcinoma cell line 8505c was from ECACC (Sigma-Aldrich, Milan, Italy), and cultured in RPMI 1640 (PAA, Pasching Austria) supplemented with 10%FBS (Sigma-Aldrich, Milan, Italy), 1% penicillin-streptomycin (Sigma-Aldrich, Milan, Italy), and 2 mM glutamine (Sigma-Aldrich, Milan, Italy).

MTS assay

For cytotoxicity assay, 8505c were plated at 1500 cells per well in triplicate in a 96-well plate (Corning, Milan, Italy). After 24 h of incubation, 1/Sil/Cur complex suspension was added ranging from 25 μ M to 0.098 μ M. After 72 h of incubation the plate was washed with sterile PBS (Sigma-Aldrich, Milan, Italy), to avoid colour interference from the compound. 20 μ L of the CellTiter 96 AQueous One Solution (Promega, Milan, Italy) was added, and the plate incubated for 4 hours at 37 °C. Absorbance at 490 nm was recorded with a plate reader (Multiskan™ TC Microplate, Thermo, Milan, Italy). Results were expressed as % of viability respect the control cells not treated.

Fluorescence microscopy

8505c cells were seeded in a Nunc Lab-Tek Chamber Slide (Nunc, Thermo, Milan, Italy) at a density of 300 000 cells per slide in RPMI 1640 (PAA, Pasching Austria) culture medium and incubated at standard conditions. After 24 hours 1/Sil/Cur complex was added at 10 μ M and incubated for 24 hours. Slides were then extensively washed with PBS-containing Ca and Mg (Sigma-Aldrich, Milan, Italy), and counterstained with Evans Blue (Sigma-Aldrich, Milan, Italy) in PBS (Sigma-Aldrich, Milan, Italy) at 0.005%. Slides were observed with a Zeiss Axiophot fluorescence microscope with a FITC filter equipped with a Nikon DS-Fi1 CCD-camera.

Conclusions

In conclusion we developed a dual drug-loaded HNT-CD glycocluster delivery system based on cyclodextrin functionalized halloysite nanotubes. These nanomaterials showed simultaneously carrier ability for two different natural drugs (silibinin and curcumin).

Release studies showed that pH affects deeply the kinetic course of the process. At different pH a complementary behavior of drugs was observed. ELLA assay showed that mannoside-cyclodextrins HNT entities displayed high affinity towards concanavalin A. The cluster effect of compound **1** has increased approximately 700-fold the relative potency of **1** compound respect to α -Me-mannoside.

In addition, the 1/Sil/Cur showed an improved cytotoxicity activity against 8505c cell lines compared to free drugs. The associated activity might be ascribed to the enhanced cellular internalization due to carbohydrate-receptor-mediated endocytosis with nuclear specific targeting. This work reported the first experimental evidence that halloysite could penetrate cellular membrane and surround cell nuclei.

Therefore the results suggest potential benefits of the use of co-administration of curcumin and silibinin in HNT-cyclodextrin glycocluster in clinical practice and could provide a promising platform for future application *in vivo*.

Acknowledgements

The work was financially supported by the University of Palermo, FIRB 2012 (prot. RBFR12ETL5) PON-TECLA (PON03PE_00214_1) and the Spanish Ministerio de Economía y Competitividad (SAF2013-44021-R). JLJB also thank Dr J. M. Benito (Instituto de investigaciones Químicas-CSIC) for his technical assistance in ELLA experiments.

Notes and references

- M. Karimi, A. Ghasemi, P. Sahandi Zangabad, R. Rahighi, S. M. Moosavi Basri, H. Mirshekari, M. Amiri, Z. Shafaei Pishabad, A. Aslani, M. Bozorgomid, D. Ghosh, A. Beyzavi, A. Vaseghi, A. R. Aref, L. Haghani, S. Bahrami and M. R. Hamblin, *Chem. Soc. Rev.*, 2016, **45**, 1457–1501.
- W. L. Lee, W. M. Guo, V. H. B. Ho, A. Saha, H. C. Chong, N. S. Tan, E. Widjaja, E. Y. Tan and S. C. J. Loo, *Small*, 2014, **10**, 3986–3996.
- F. Ahmed, R. I. Pakunlu, A. Brannan, F. Bates, T. Minko and D. E. Discher, *J. Controlled Release*, 2006, **116**, 150–158.
- A. Datt, I. El-Maazawi and S. C. Larsen, *J. Phys. Chem. C*, 2012, **116**, 18358–18366.
- P. Pasbakhsh, G. J. Churchman and J. L. Keeling, *Appl. Clay Sci.*, 2013, **74**, 47–57.
- T. G. Shutava, R. F. Fakhrullin and Y. M. Lvov, *Curr. Opin. Pharmacol.*, 2014, **18**, 141–148.
- Y. Lvov and E. Abdullayev, *Prog. Polym. Sci.*, 2013, **38**, 1690–1719.
- P. Yuan, P. D. Southon, Z. Liu, M. E. R. Green, J. M. Hook, S. J. Antill and C. J. Kepert, *J. Phys. Chem. C*, 2008, **112**, 15742–15751.
- M. Liu, R. He, J. Yang, W. Zhao and C. Zhou, *ACS Appl. Mater. Interfaces*, 2016, **8**, 7709–7719.
- M. Liu, C. Wu, Y. Jiao, S. Xiong and C. Zhou, *J. Mater. Chem. B*, 2013, **1**, 2078–2089.
- G. I. Fakhrullina, F. S. Akhatova, Y. M. Lvov and R. F. Fakhrullin, *Environ. Sci.: Nano*, 2015, **2**, 54–59.
- E. A. Naumenko, I. D. Guryanov, R. Yendluri, Y. M. Lvov and R. F. Fakhrullin, *Nanoscale*, 2016, **8**, 7257–7271.
- M. Kryuchkova, A. Danilushkina, Y. Lvov and R. Fakhrullin, *Environ. Sci.: Nano*, 2016, **3**, 442–452.
- L. Bellani, L. Giorgetti, S. Riela, G. Lazzara, A. Scialabba and M. Massaro, *Environ. Toxicol. Chem.*, 2016, DOI: 10.1002/etc.3412.
- Y. Lvov, W. Wang, L. Zhang and R. Fakhrullin, *Adv. Mater.*, 2016, **28**, 1227–1250.
- R. R. Price, B. P. Gaber and Y. Lvov, *J. Microencapsulation*, 2001, **18**, 713–722.
- M. Massaro, R. Amorati, G. Cavallaro, S. Guernelli, G. Lazzara, S. Milioto, R. Noto, P. Poma and S. Riela, *Colloids Surf., B*, 2016, **140**, 505–513.
- Y. M. Lvov, M. M. DeVilliers and R. F. Fakhrullin, *Expert Opin. Drug Delivery*, 2016, **13**, 977–986.
- M. Massaro, S. Riela, S. Guernelli, F. Parisi, G. Lazzara, A. Baschieri, L. Valgimigli and R. Amorati, *J. Mater. Chem. B*, 2016, **4**, 2229–2241.
- D. Tan, P. Yuan, F. Annabi-Bergaya, D. Liu, L. Wang, H. Liu and H. He, *Appl. Clay Sci.*, 2014, **96**, 50–55.
- L. Fan, B. Li, Q. Wang, A. Wang and J. Zhang, *Adv. Mater. Interfaces*, 2014, **1**, 1300136.
- M. Liu, Y. Chang, J. Yang, Y. You, R. He, T. Chen and C. Zhou, *J. Mater. Chem. B*, 2016, **4**, 2253–2263.
- M. R. Dзамukova, E. A. Naumenko, Y. M. Lvov and R. F. Fakhrullin, *Sci. Rep.*, 2015, **5**, 10560.
- C. Aguzzi, C. Viseras, P. Cerezo, I. Salcedo, R. Sánchez-Espejo and C. Valenzuela, *Colloids Surf., B*, 2013, **105**, 75–80.
- X. Li, Q. Yang, J. Ouyang, H. Yang and S. Chang, *Appl. Clay Sci.*, 2016, **126**, 306–312.
- D. Tan, P. Yuan, F. Annabi-Bergaya, F. Dong, D. Liu and H. He, *Appl. Clay Sci.*, 2015, **114**, 190–196.
- X. Zhang, R. Guo, J. Xu, Y. Lan, Y. Jiao, C. Zhou and Y. Zhao, *J. Biomater. Appl.*, 2015, **30**, 512–525.
- M. Massaro, S. Piana, C. G. Colletti, R. Noto, S. Riela, C. Baiamonte, C. Giordano, G. Pizzolanti, G. Cavallaro, S. Milioto and G. Lazzara, *J. Mater. Chem. B*, 2015, **3**, 4074–4081.
- M. Massaro, C. G. Colletti, R. Noto, S. Riela, P. Poma, S. Guernelli, F. Parisi, S. Milioto and G. Lazzara, *Int. J. Pharm.*, 2015, **478**, 476–485.
- S. Riela, M. Massaro, C. G. Colletti, A. Bommarito, C. Giordano, S. Milioto, R. Noto, P. Poma and G. Lazzara, *Int. J. Pharm.*, 2014, **475**, 613–623.
- M. Guo, A. Wang, F. Muhammad, W. Qi, H. Ren, Y. Guo and G. Zhu, *Chin. J. Chem.*, 2012, **30**, 2115–2120.
- M. Gómez-García, J. M. Benito, A. P. Butera, C. O. Mellet, J. M. G. Fernández and J. L. J. Blanco, *J. Org. Chem.*, 2012, **77**, 1273–1288.
- M. Gomez-Garcia, J. M. Benito, R. Gutierrez-Gallego, A. Maestre, C. O. Mellet, J. M. G. Fernandez and J. L. J. Blanco, *Org. Biomol. Chem.*, 2010, **8**, 1849–1860.
- M. Massaro, S. Riela, P. Lo Meo, R. Noto, G. Cavallaro, S. Milioto and G. Lazzara, *J. Mater. Chem. B*, 2014, **2**, 7732–7738.
- V. S. Bollu, A. K. Barui, S. K. Mondal, S. Prashar, M. Fajardo, D. Briones, A. Rodríguez-Díéguez, C. R. Patra and S. Gómez-Ruiz, *Mater. Sci. Eng., C*, 2016, **63**, 393–410.
- Z. Zhang, R. Zhang, L. Zou, L. Chen, Y. Ahmed, W. Al Bishri, K. Balamash and D. J. McClements, *Food Hydrocolloids*, 2016, **58**, 160–170.
- S. Kim, J. Han, M. Jeon, D. You, J. Lee, H. J. Kim, S. Bae, S. J. Nam and J. E. Lee, *Tumor Biol.*, 2016, 1–11, DOI: 10.1007/s13277-016-5000-7.
- G. Cavallaro, G. Lazzara and S. Milioto, *J. Phys. Chem. C*, 2012, **116**, 21932–21938.
- M. Massaro, S. Riela, G. Cavallaro, C. G. Colletti, S. Milioto, R. Noto and G. Lazzara, *ChemistrySelect*, 2016, **1**, 1773–1779.
- J. Zhu, H. He, L. Zhu, X. Wen and F. Deng, *J. Colloid Interface Sci.*, 2005, **286**, 239–244.

- 41 M. Du, B. Guo and D. Jia, *Eur. Polym. J.*, 2006, **42**, 1362–1369.
- 42 Z. Xu, S. Liu, Y. Kang and M. Wang, *Nanoscale*, 2015, **7**, 5859–5868.
- 43 J.-H. Park, L. Gu, G. von Maltzahn, E. Ruoslahti, S. N. Bhatia and M. J. Sailor, *Nat. Mater.*, 2009, **8**, 331–336.
- 44 B. Tang, L. Ma, H.-y. Wang and G.-y. Zhang, *J. Agric. Food Chem.*, 2002, **50**, 1355–1361.
- 45 H.-Z. Ouyang, L. Fang, L. Zhu, L. Zhang, X.-L. Ren, J. He and A.-D. Qi, *J. Inclusion Phenom. Macrocyclic Chem.*, 2011, **73**, 423–433.
- 46 A. Wilczak and T. M. Keinath, *Water Environ. Res.*, 1993, **65**, 238–244.
- 47 J. Siepmann and N. A. Peppas, *Adv. Drug Delivery Rev.*, 2001, **48**, 139–157.
- 48 M. Ragazzi, A. Ciarrocchi, V. Sancisi, G. Gandolfi, A. Bisagni and S. Piana, *Int. J. Endocrinol.*, 2014, **2014**, 13.